Supplementary material for

Tetracoordinated copper(I) complexes featuring aggregation-induced emission characteristics for sensitive detection of mercury ions

Yi-Hao Zheng, Hong-Yi Liu, Han-Lu Qin, Peng-Xin Bai, Hong-Yan Li*

School of Chemical Engineering and Technology, Hebei University of Technology, Tianjin 300401, China

* Corresponding author.

E-mail address: hyli@hebut.edu.cn (H.-Y. Li)

Contents

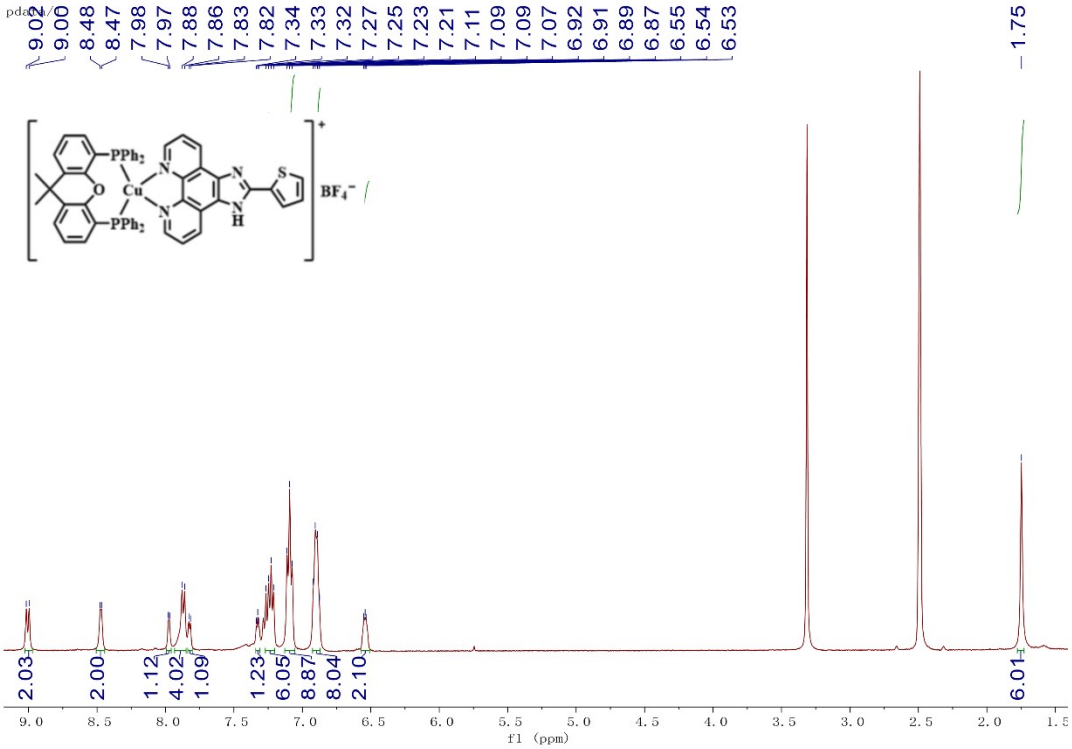

Fig. S1 ^{1}H NMR spectrum of **Cu1** in DMSO-d_6 at room temperature.

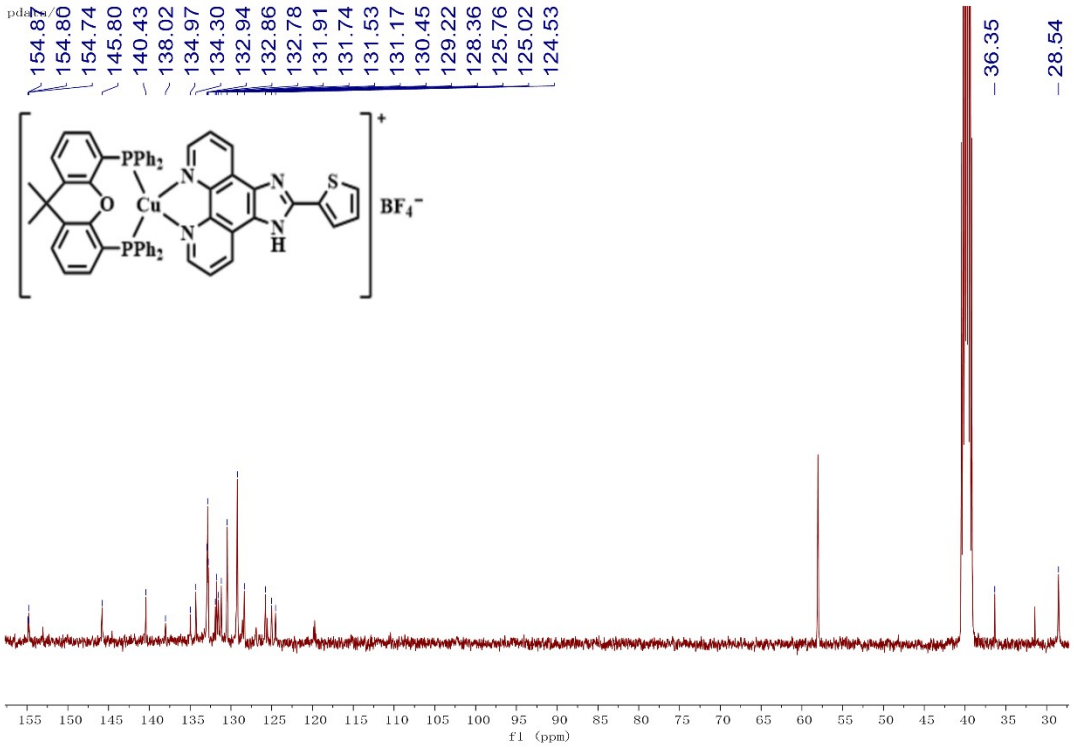

Fig. S2 ^{13}C NMR spectrum of **Cu1** in DMSO-d_6 at room temperature.

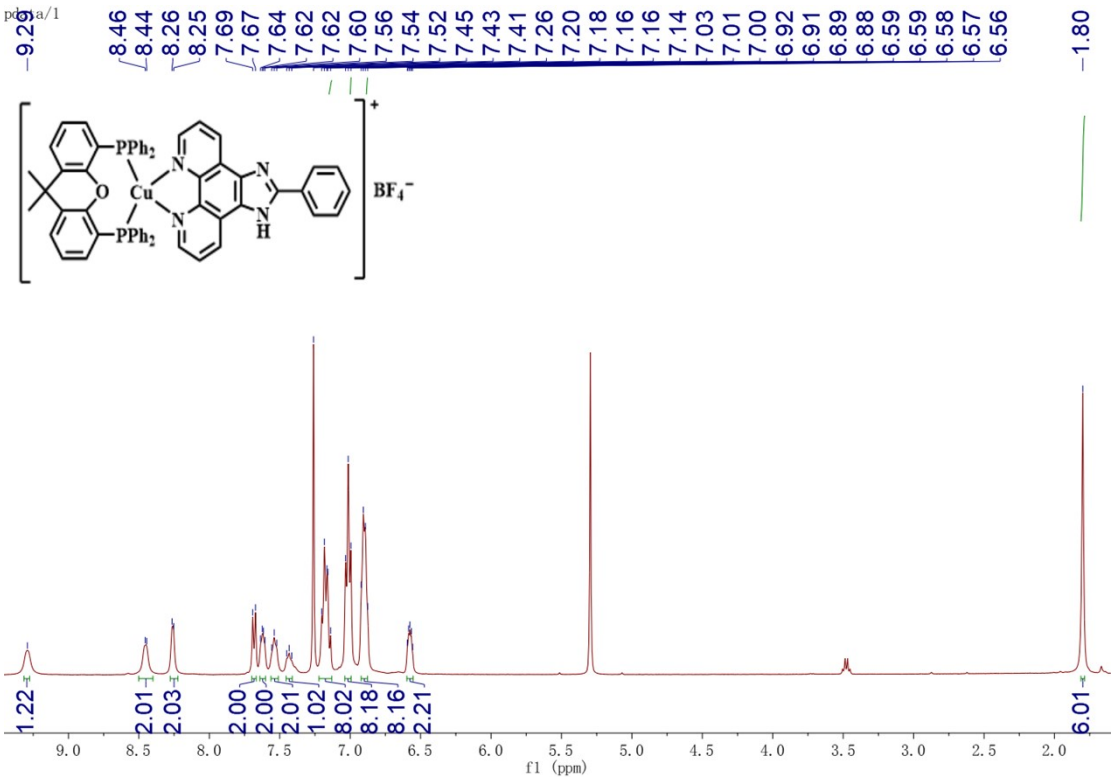

Fig. S3 ^{1}H NMR spectrum of **Cu2** in $CDCl_3$ at room temperature.

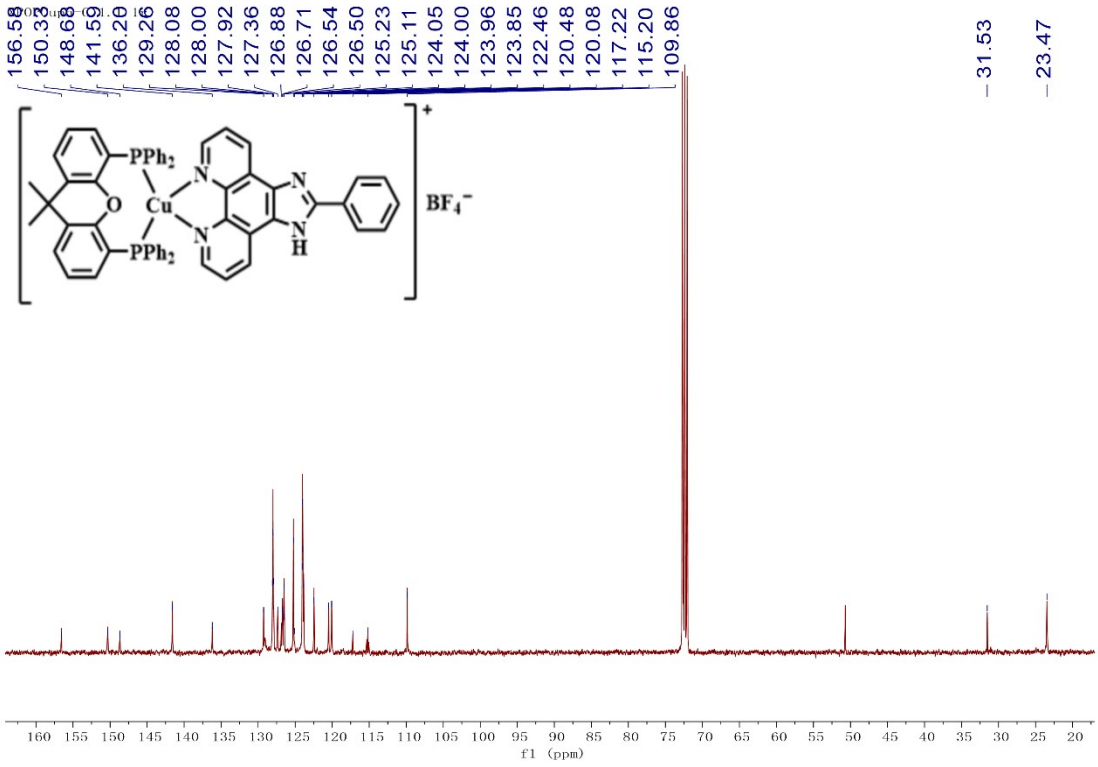

Fig. S4 ^{13}C NMR spectrum of **Cu2** in $CDCl_3$ at room temperature.

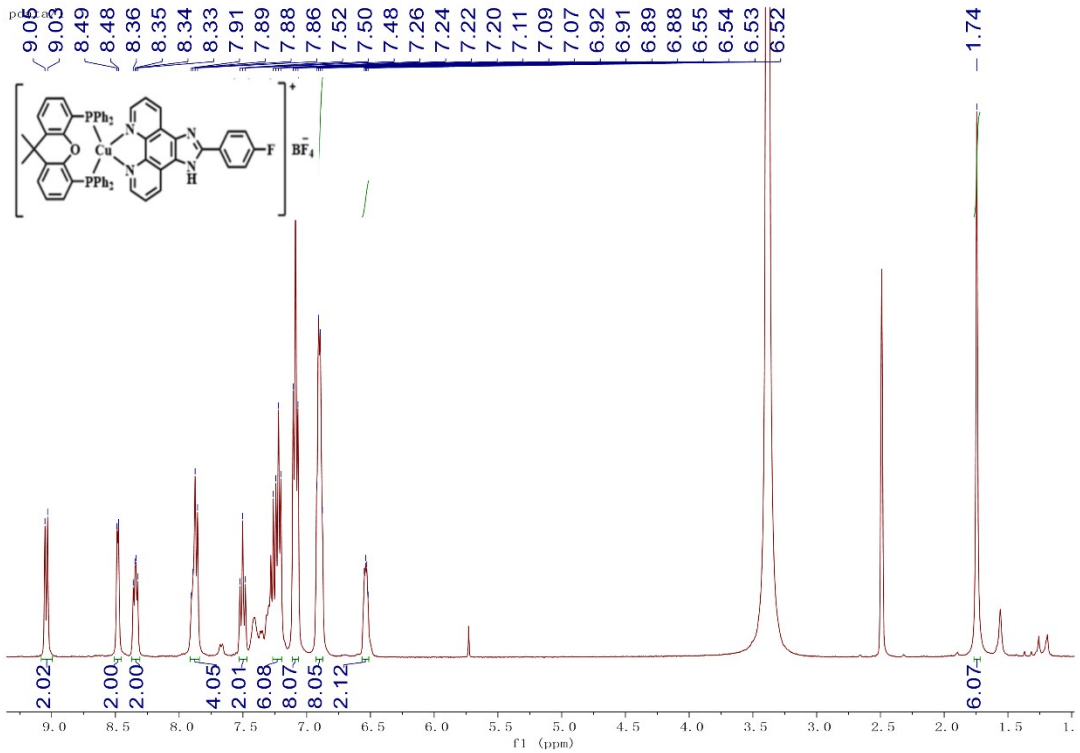

Fig. S5 ^{1}H NMR spectrum of **Cu3** in DMSO-d_6 at room temperature.

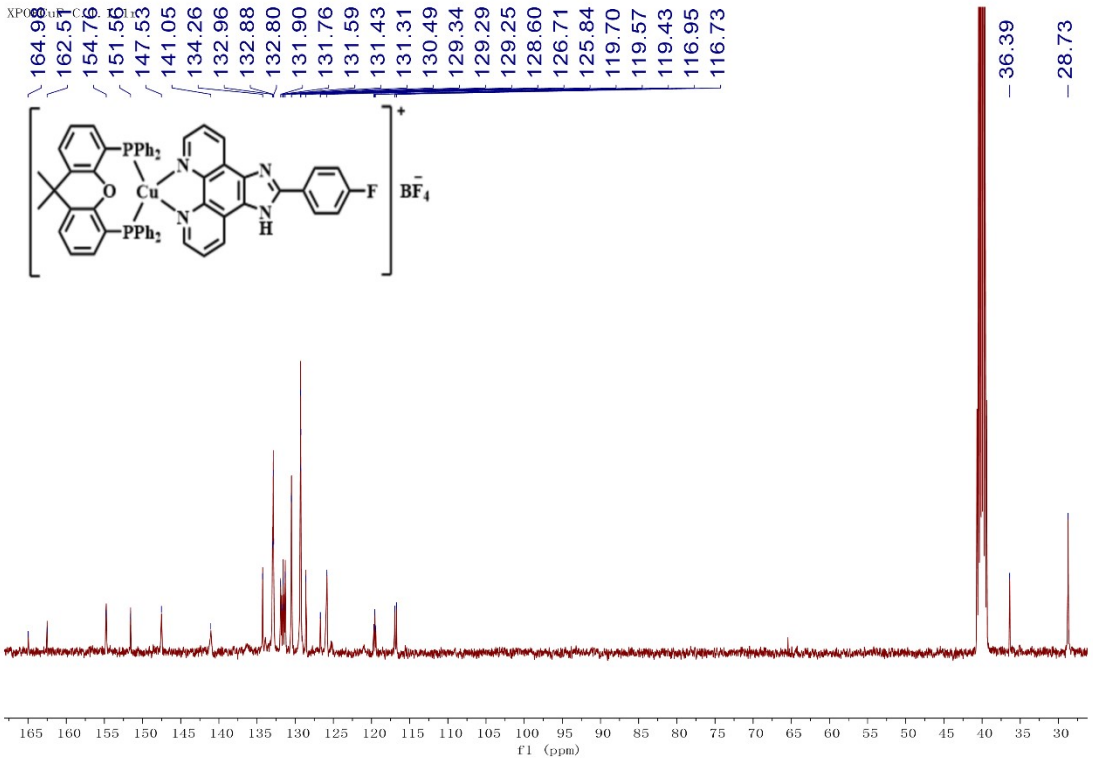

Fig. S6 ^{13}C NMR spectrum of **Cu3** in DMSO-d_6 at room temperature.

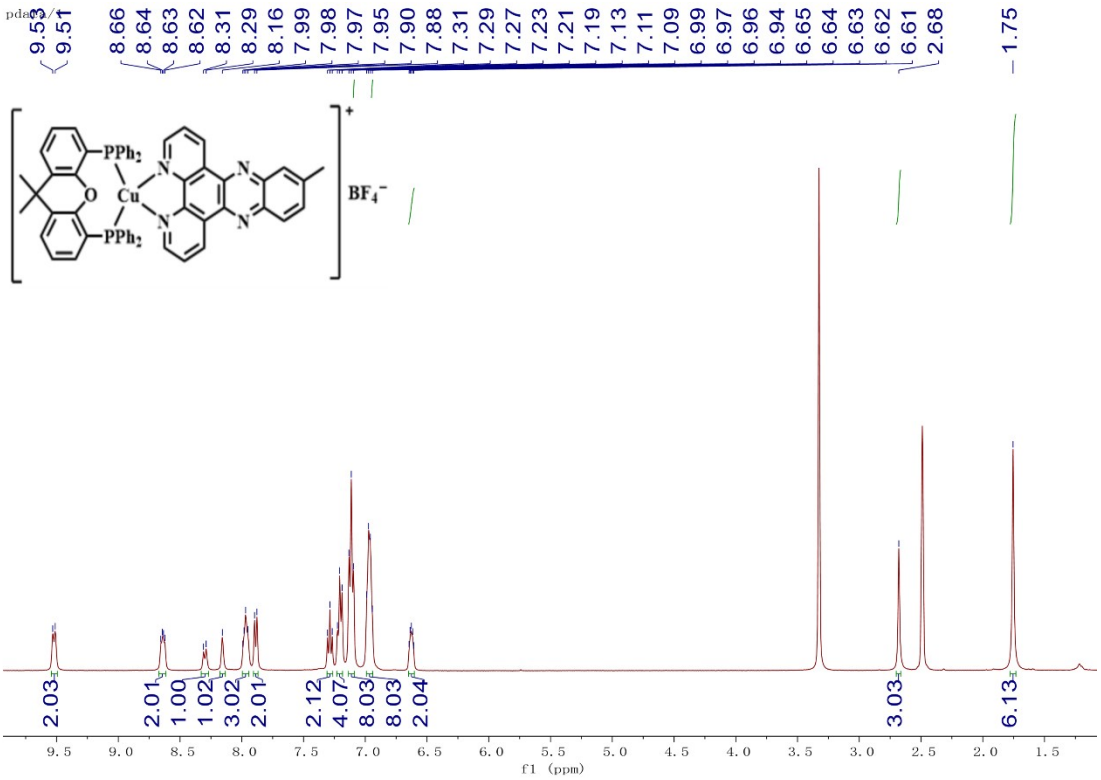

Fig. S7 ^{1}H NMR spectrum of **Cu4** in DMSO-d_6 at room temperature.

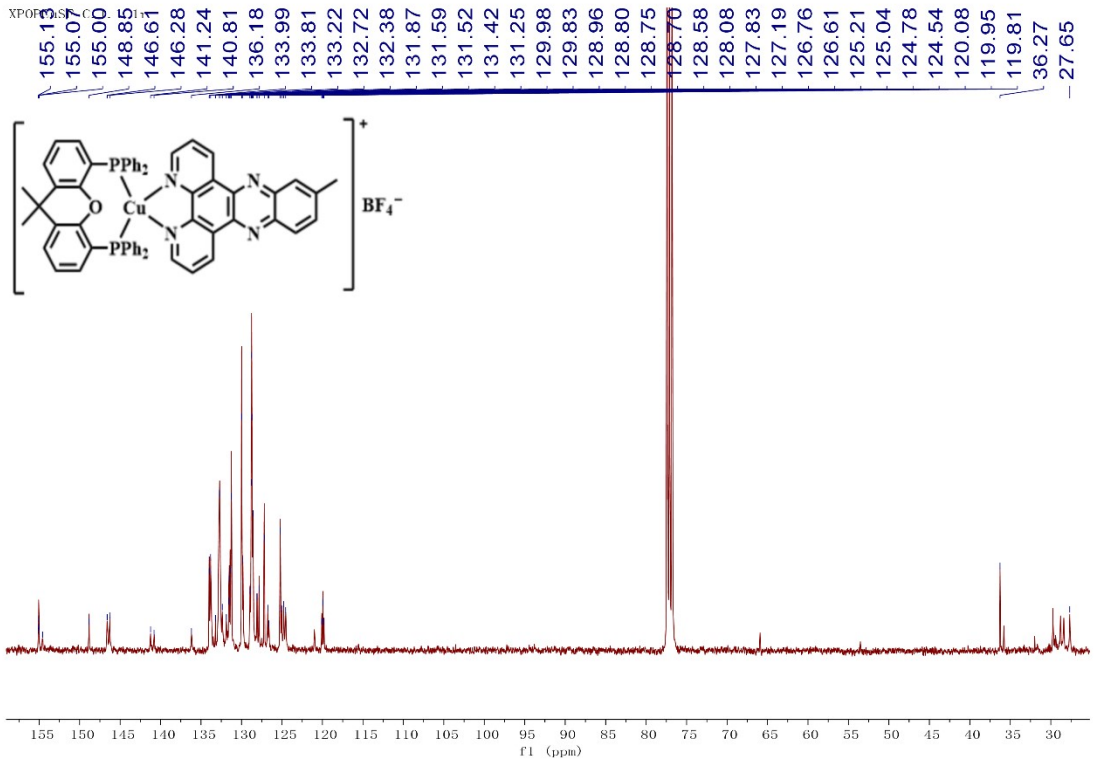

Fig. S8 ^{13}C NMR spectrum of **Cu4** in DMSO-d_6 at room temperature.

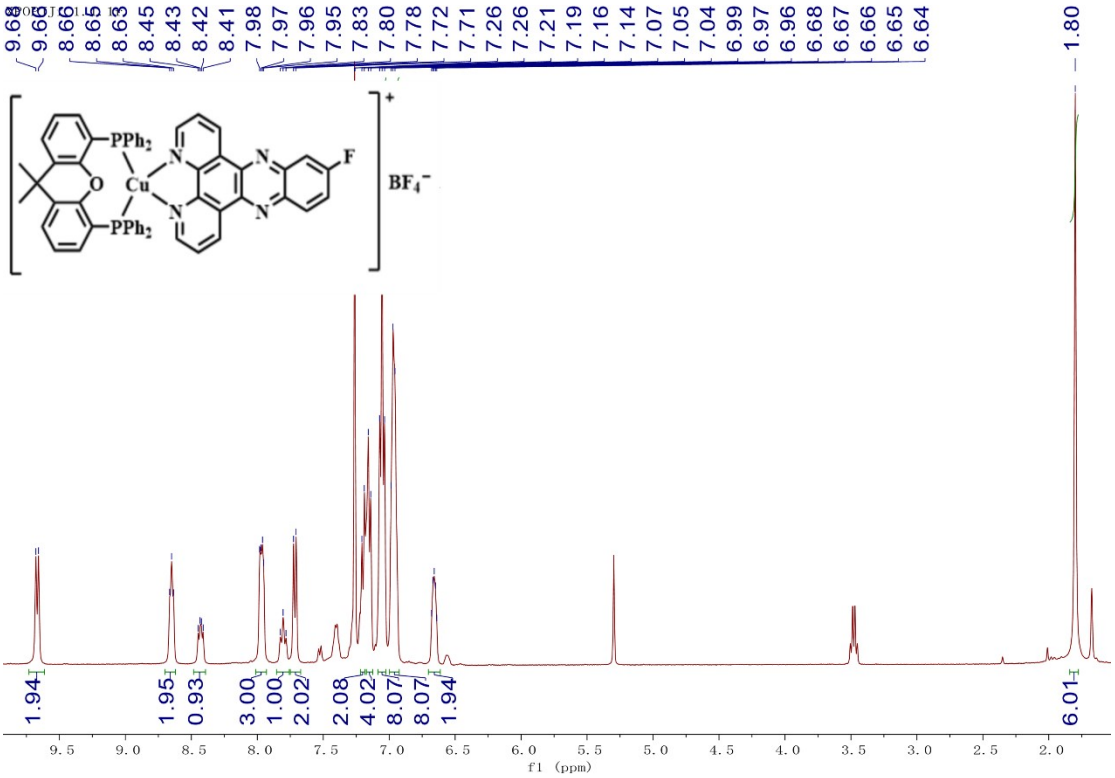

Fig. S9 ^{1}H NMR spectrum of **Cu5** in DMSO-d_6 at room temperature.

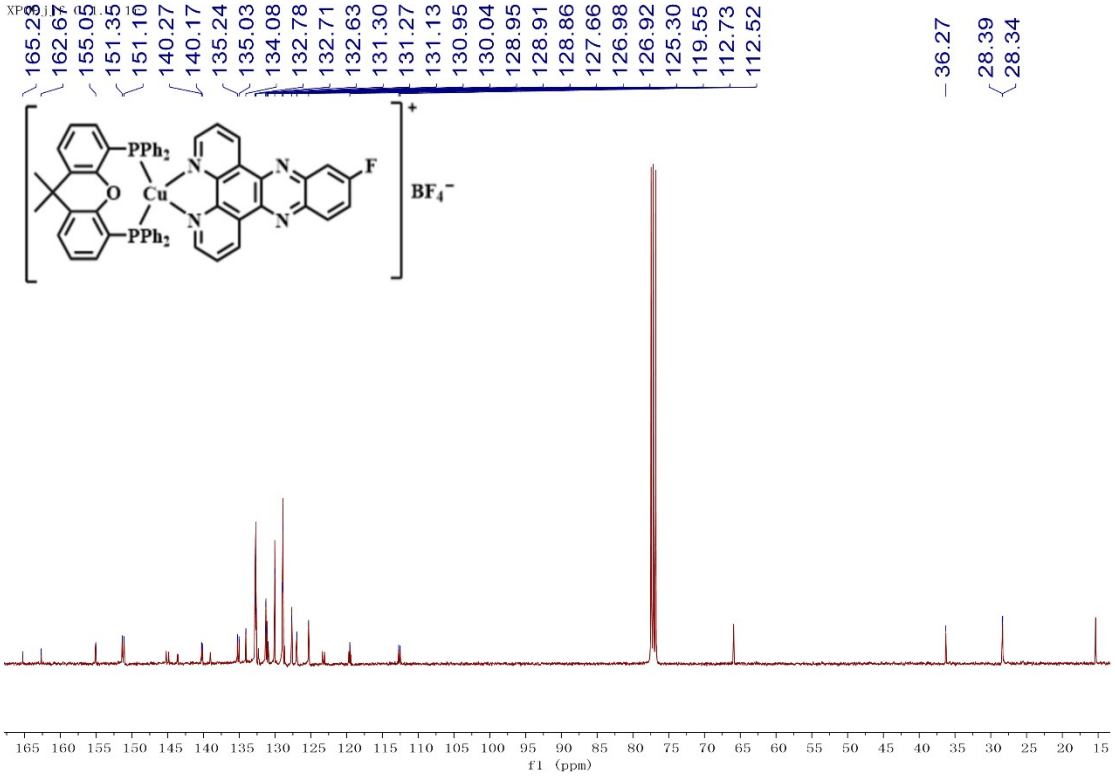

Fig. S10 ^{13}C NMR spectrum of **Cu5** in DMSO-d_6 at room temperature.

h6h6

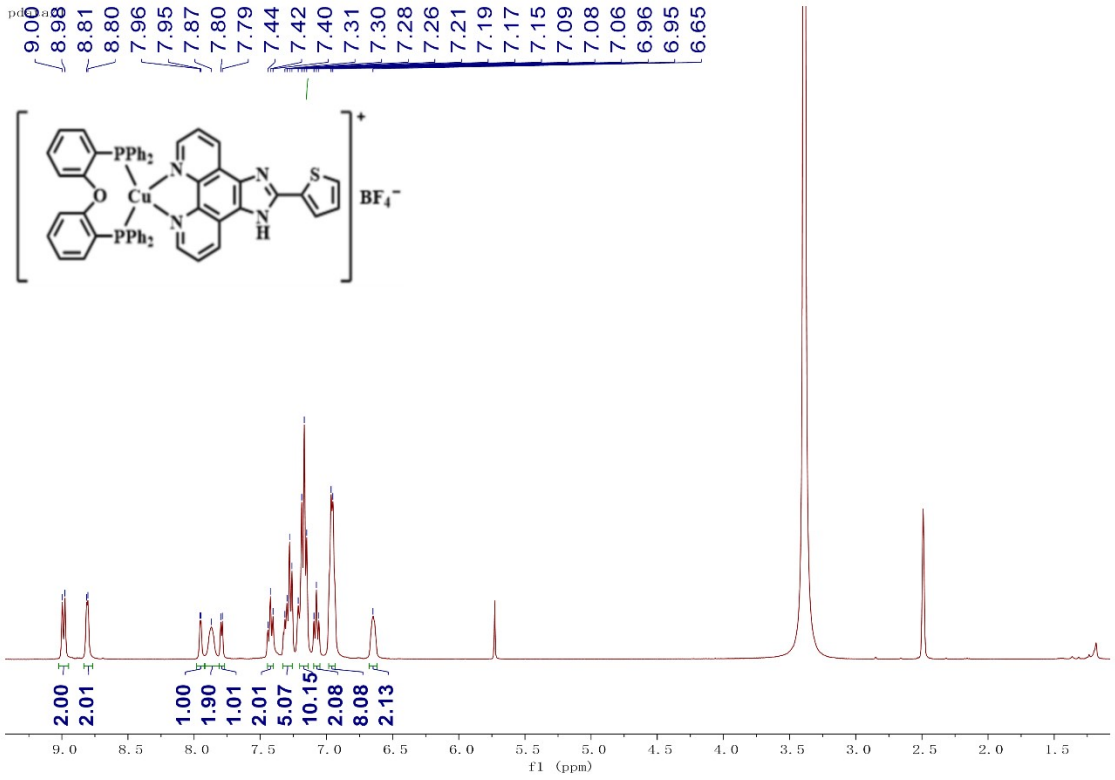

Fig. S11 ^{1}H NMR spectrum of **Cu6** in DMSO-d_6 at room temperature.

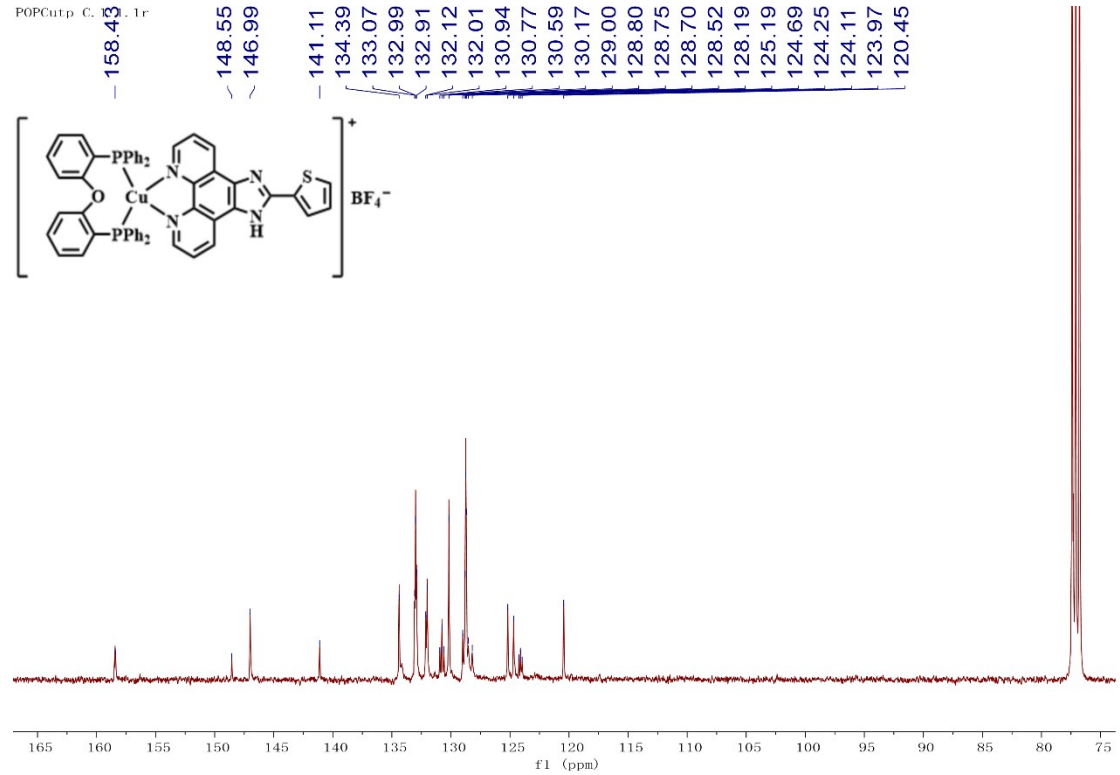

Fig. S12 ^{13}C NMR spectrum of **Cu6** in DMSO-d_6 at room temperature.

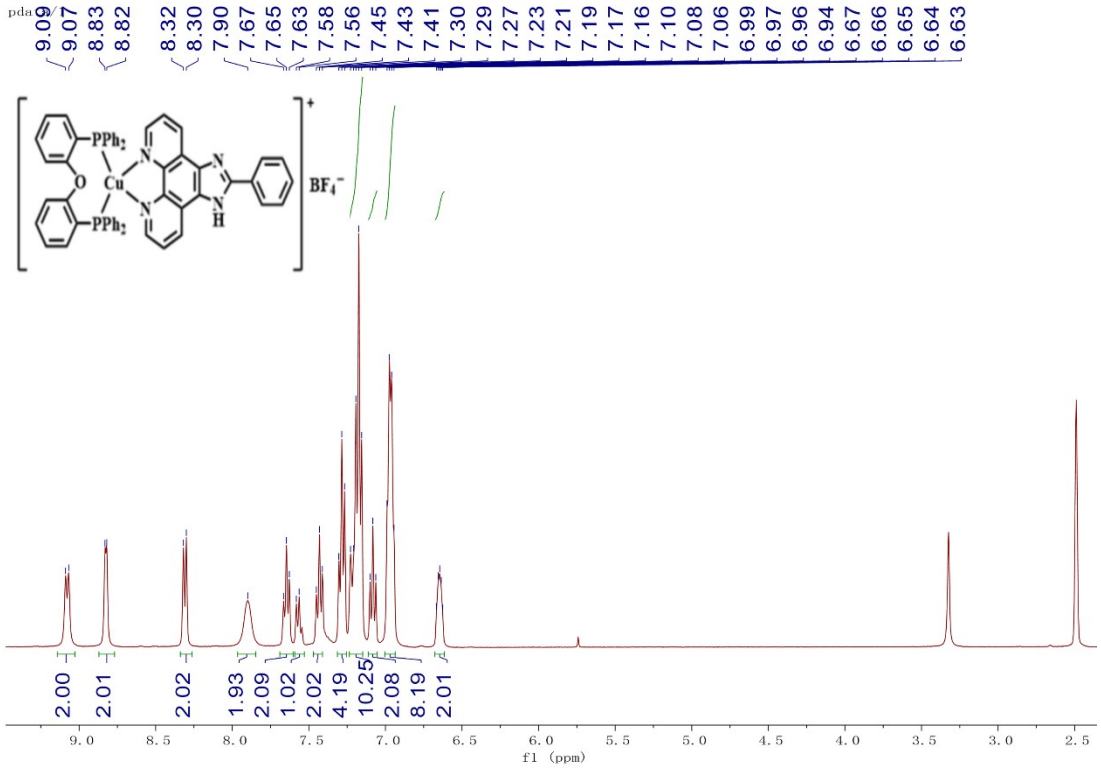

Fig. S13 ^{1}H NMR spectrum of **Cu7** in DMSO-d_6 at room temperature.

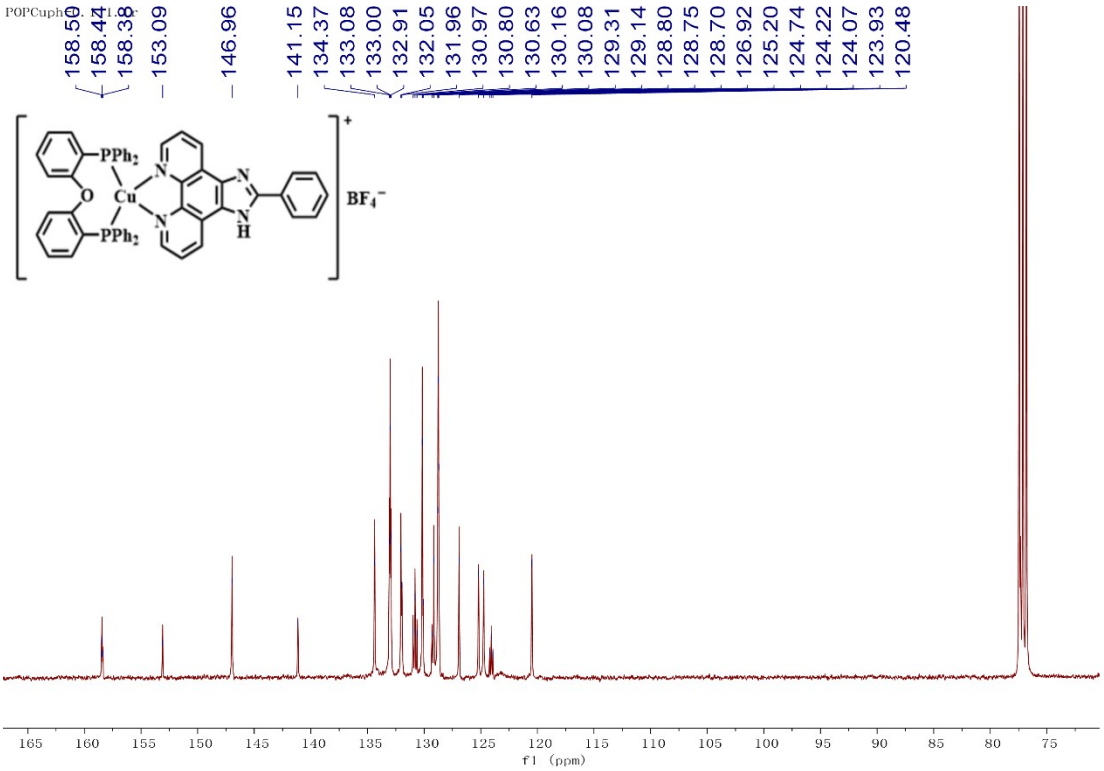

Fig. S14 ^{13}C NMR spectrum of **Cu7** in DMSO-d_6 at room temperature.

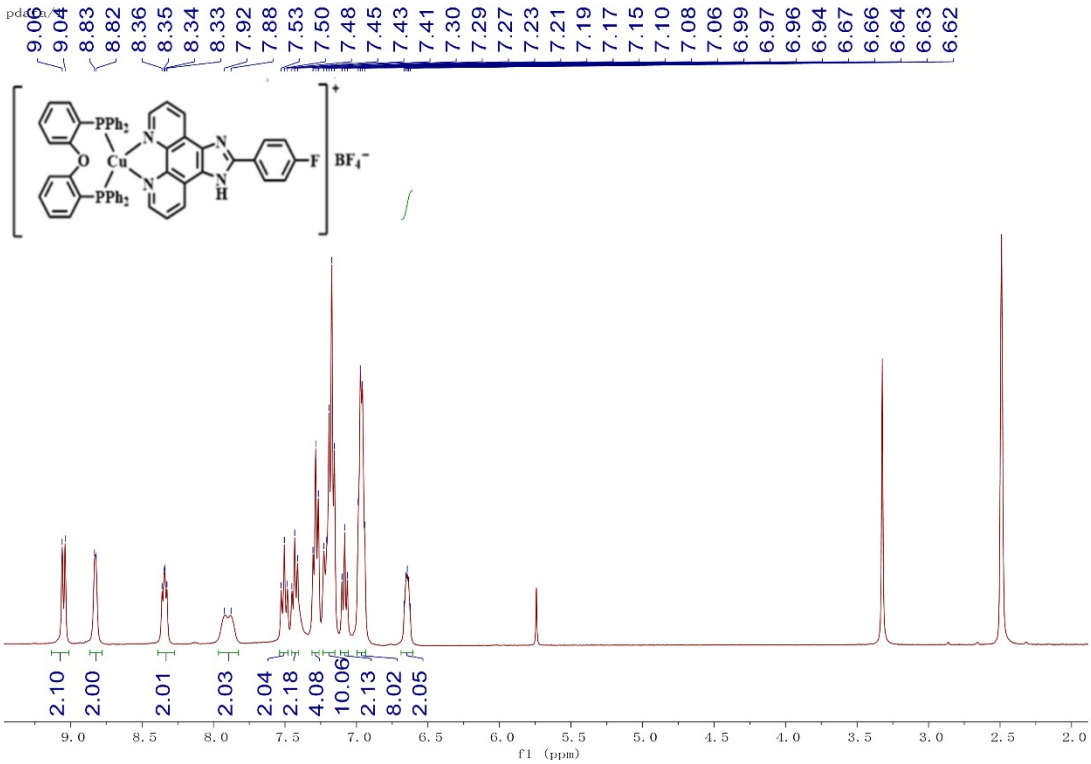

Fig. S15 ^{1}H NMR spectrum of **Cu8** in DMSO-d_6 at room temperature.

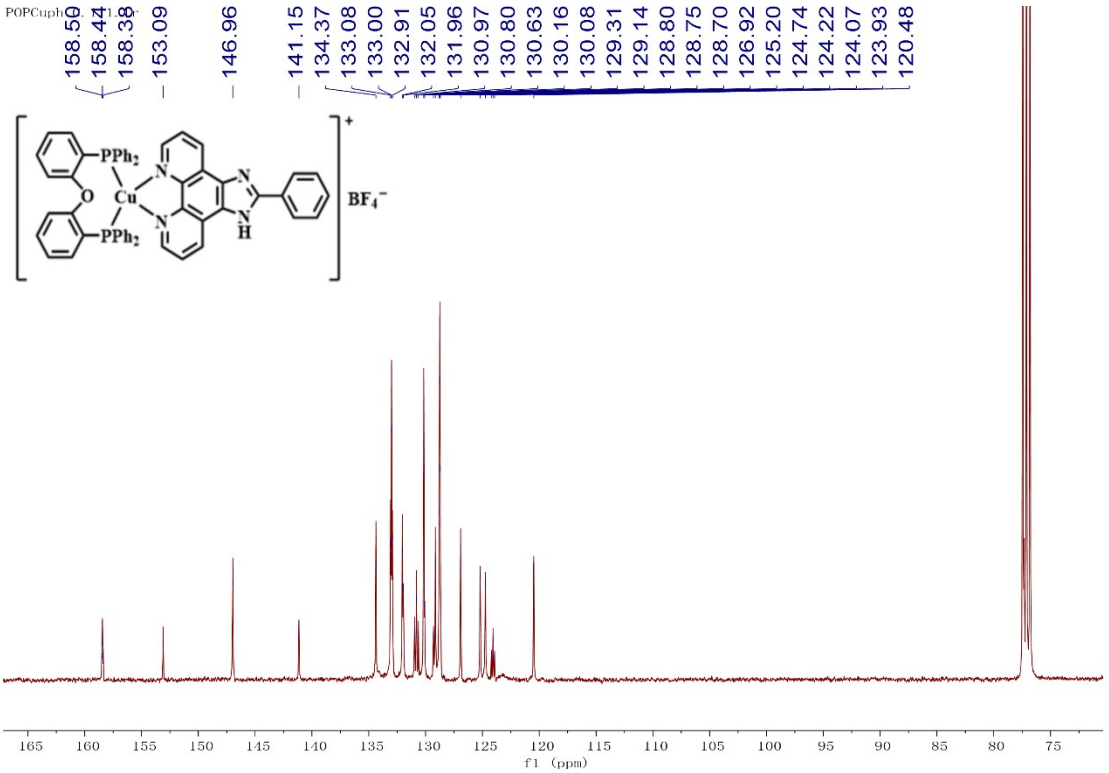

Fig. S16 ^{13}C NMR spectrum of **Cu8** in DMSO-d_6 at room temperature.

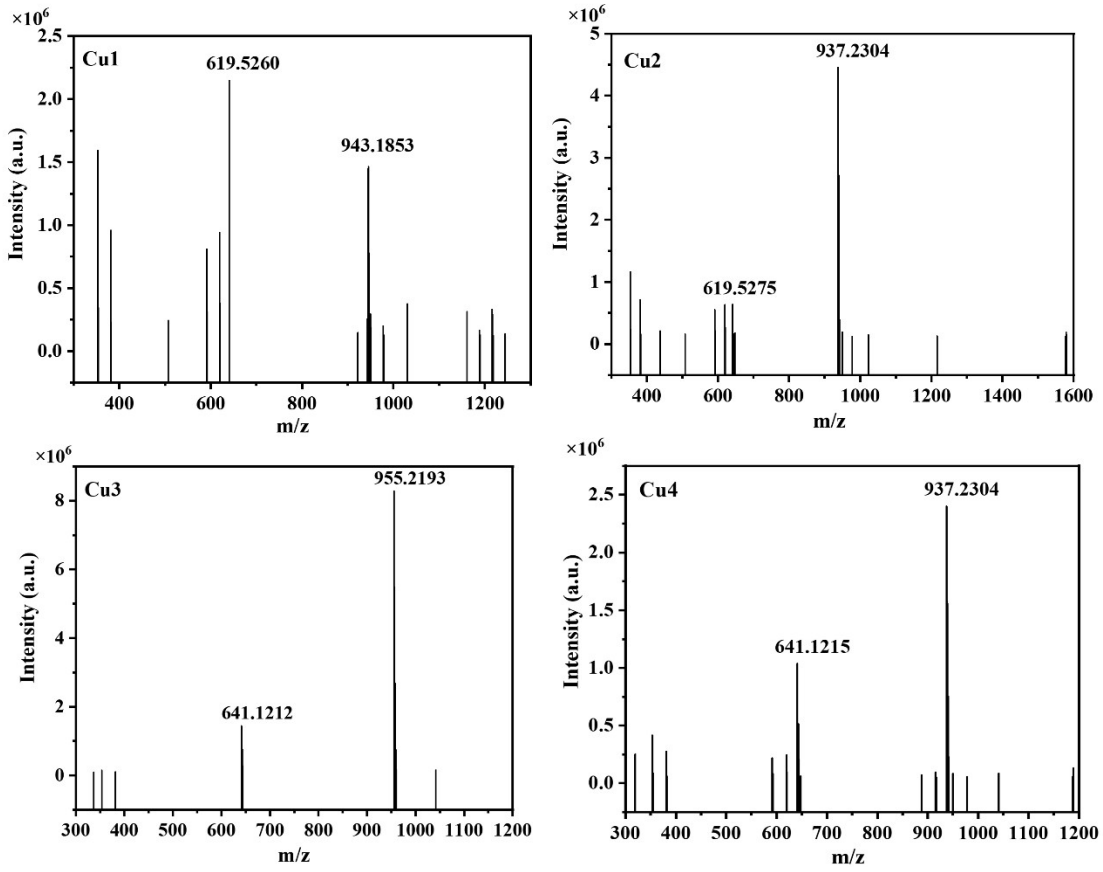

Fig. S17 The ESI-MS spectra of complexes **Cu1**–**Cu4**.

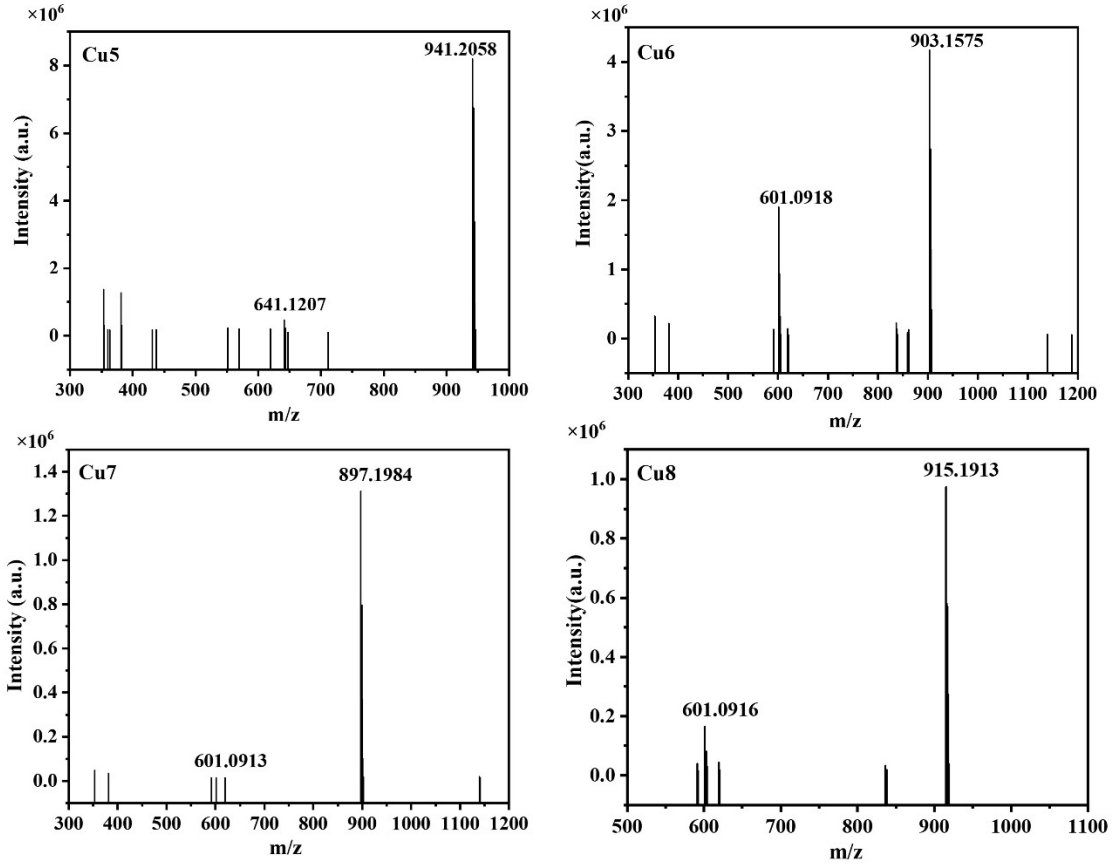

Fig. S18 The ESI-MS spectra of complexes **Cu5**–**Cu8**.

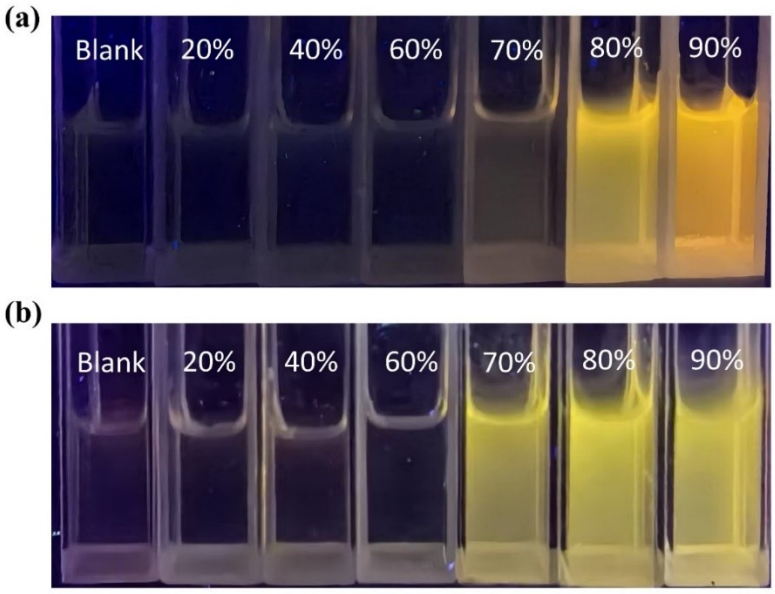

Fig. S19 The photoluminescence images of **Cu1** (a) and **Cu6** (b) under 365 nm in different water content conditions (CH_3CN/water).

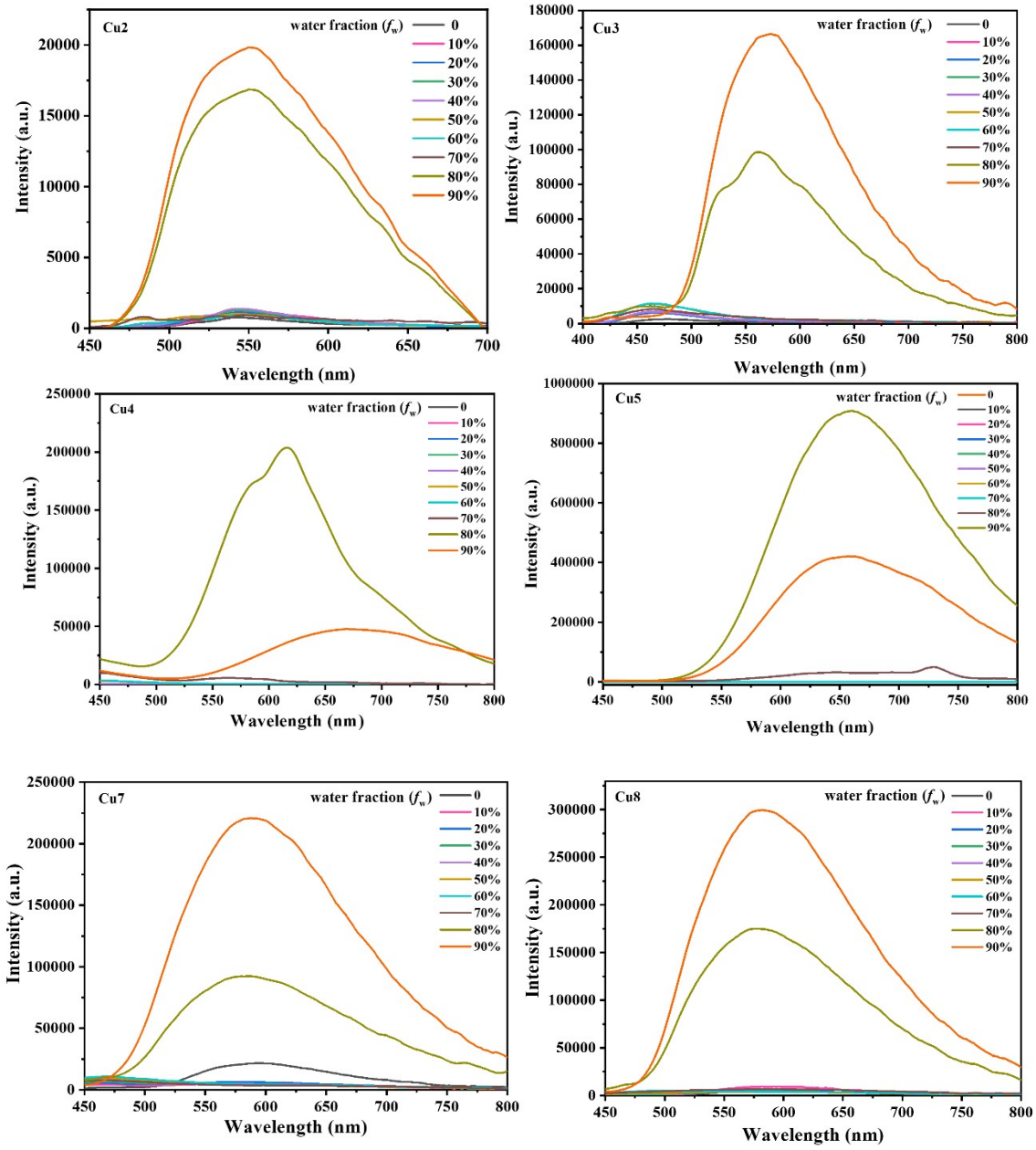

Fig. S20 PL spectra of complexes **Cu2**–**Cu5**, **Cu7**–**Cu8** in CH_3CN/H_2O mixtures with varying water fractions (f_w) (λ_{ex} = 370 nm).

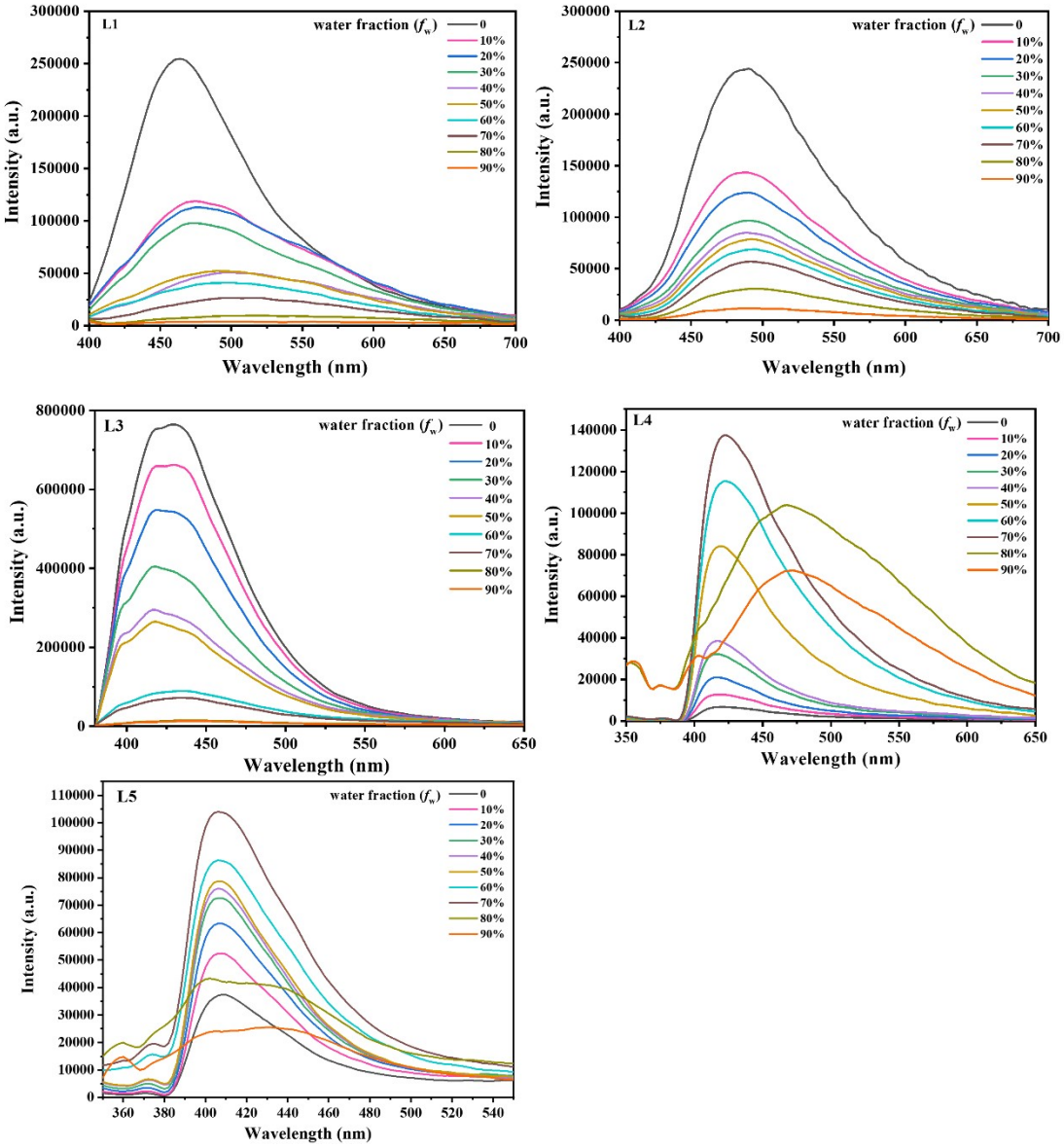

Fig. S21 PL spectra of L1–L5 in EtOH/H_2O mixtures with varying water fractions (f_w) (λ_{ex} = 370 nm).

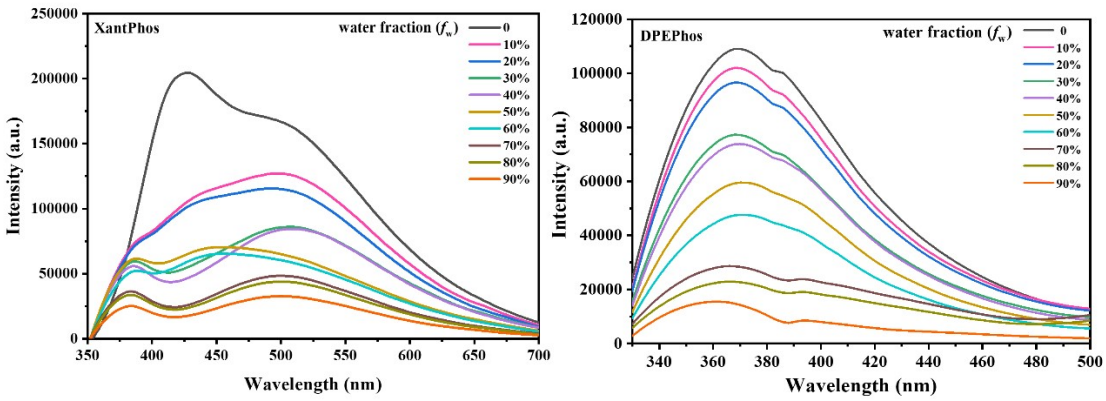

Fig. S22 PL spectra of XantPhos and DPEPhos in THF/H_2O mixtures with varying water fractions (f_w) (λ_{ex} = 370 nm).

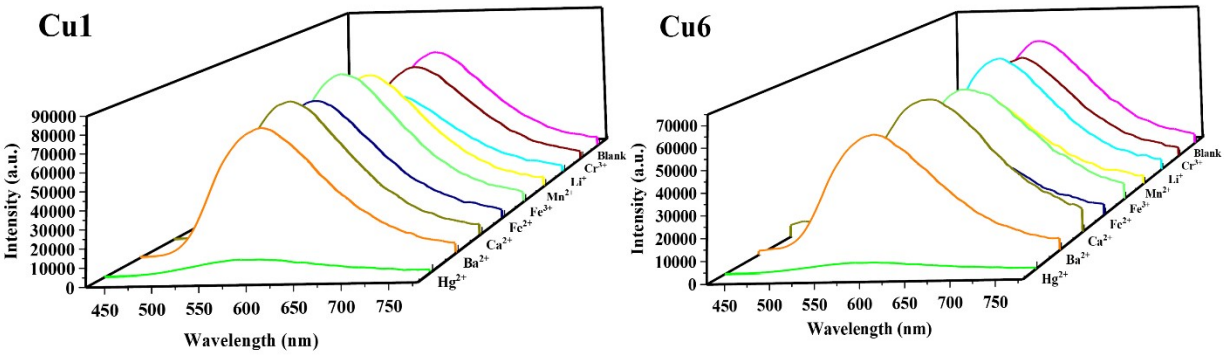

Fig. S23 PL spectra of complexes **Cu1**(a) and **Cu6** (b) (2.5 ×10^{-5} M) in the presence of different metal ions (Hg^{2+}, Ba^{2+}, Ca^{2+}, Fe^{2+}, Fe^{3+}, Mn^{2+}, Li^{+} and Cr^{3+}) under an excitation wavelength of 370 nm.

(a)

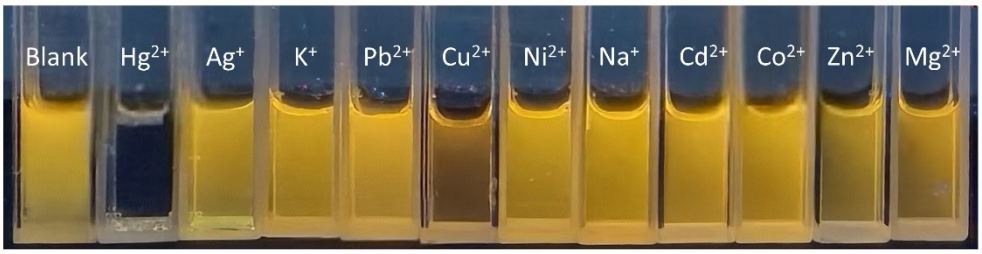

(b)

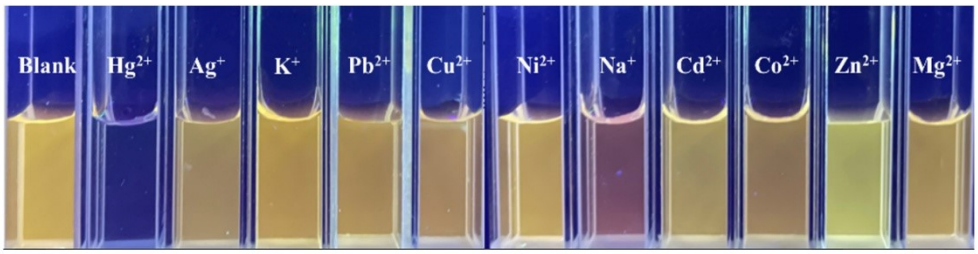

Fig. S24 The luminescence images of **Cu1** (a) and **Cu6** (b) under 365 nm ultraviolet light after the addition of different metal ions.

(a)

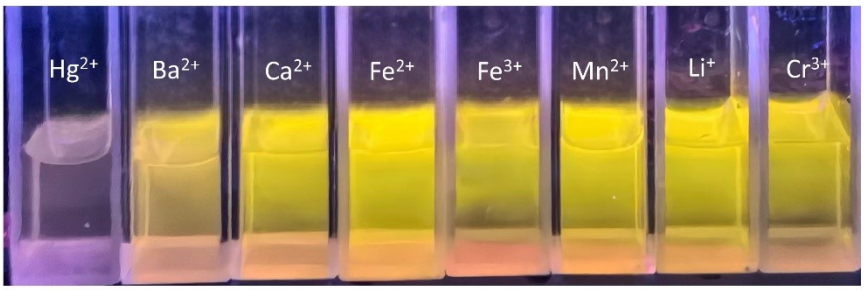

(b)

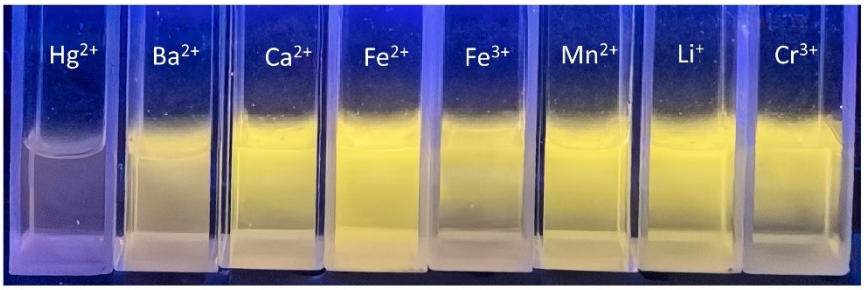

Fig. S25 The luminescence images of **Cu1** (a) and **Cu6** (b) under 365 nm ultraviolet light after the addition of different metal ions including Hg^{2+}, Ba^{2+}, Ca^{2+}, Fe^{2+}, Fe^{3+}, Mn^{2+}, Li^{+} and Cr^{3+}.

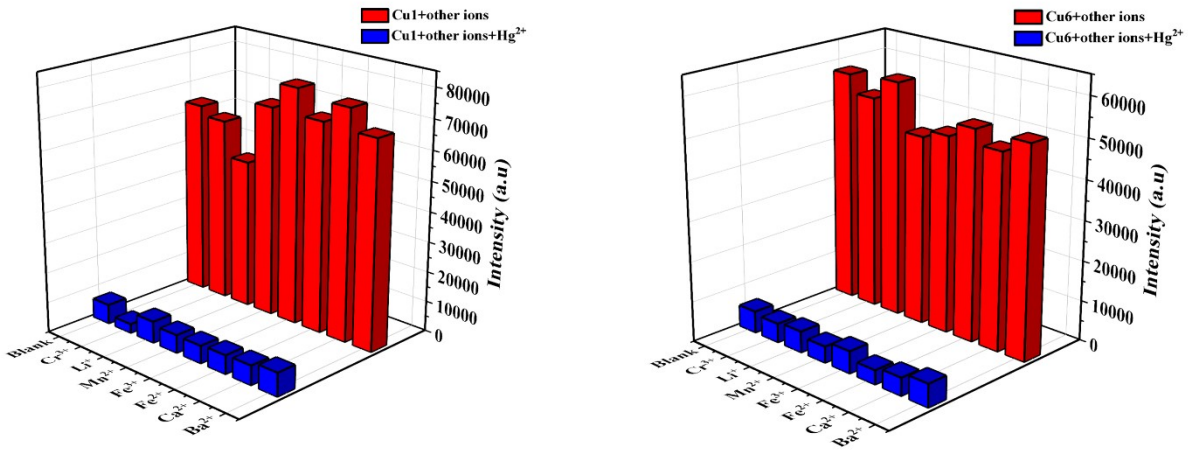

Fig. S26 PL spectra of complexes **Cu1** (a) and **Cu6** (b) (2.5×10^{-5} M) were monitored in a CH_3CN/H_2O mixture in the presence of competing metal ions (Hg^{2+}, Ba^{2+}, Ca^{2+}, Fe^{2+}, Fe^{3+}, Mn^{2+}, Li^{+} and Cr^{3+}) under an excitation wavelength of 370 nm.

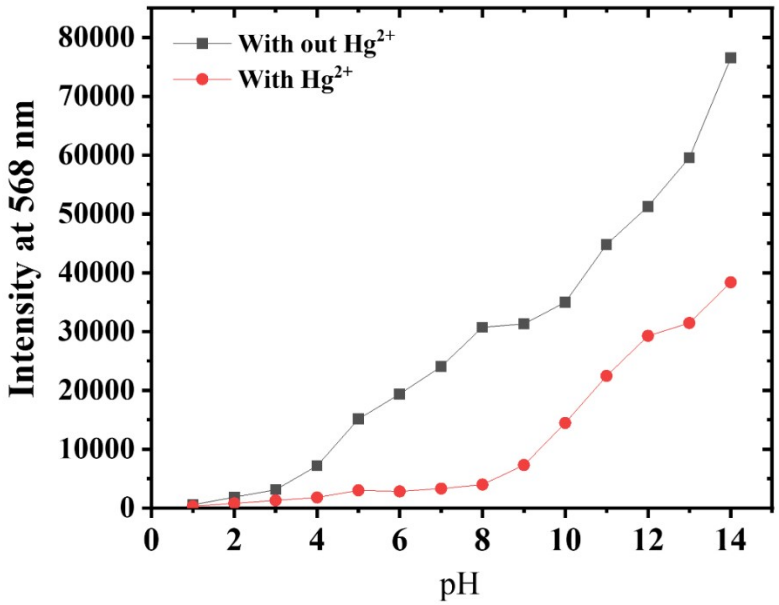

Fig. S27 The PL spectrum of complex **Cu6** in the CH_3CN/H_2O mixed solution varies with the pH value.

Table S1. Frontier orbital energy and electron density distribution for **Cu1**–**Cu8**.

Complex	Orbital	Energy (eV) (Calculated)	Composition %		
			Diphosphine ligands	Cu	Diimine ligands
Cu1	HOMO	−7.66	22.22	16.85	60.93
	LUMO	−4.17	3.25	3.27	93.48
Cu2	HOMO	−7.73	41.82	30.96	27.22
	LUMO	−4.16	3.30	3.40	93.30
Cu3	HOMO	−7.77	39.12	29.05	31.83
	LUMO	−4.16	3.31	3.41	93.28
Cu4	HOMO	−7.80	56.85	39.39	3.75
	LUMO	−4.57	0.71	0.28	99.01
Cu5	HOMO	−7.86	57.00	17.61	25.39
	LUMO	−4.76	3.36	3.29	93.35
Cu6	HOMO	−7.68	47.77	31.98	20.25
	LUMO	−4.22	3.42	3.42	93.16
Cu7	HOMO	−7.72	45.49	30.54	23.96
	LUMO	−4.22	3.42	3.43	93.16
Cu8	HOMO	−7.74	54.04	35.47	10.49
	LUMO	−4.22	3.22	3.00	93.79

Table S2. Major experimental and calculated optical transitions for **Cu1**–**Cu8**.

Complex	Orbital Excitation	Transitions	Oscillation strength	Calcd (nm)	Exptl (nm)
Cu1	HOMO→LUMO	MLCT/LLCT	0.19	407	413
Cu2	HOMO→LUMO	MLCT/LLCT	0.17	400	411
Cu3	HOMO→LUMO	MLCT/LLCT	0.36	401	408
Cu4	HOMO→LUMO	MLCT/LLCT	0.08	420	415
Cu5	HOMO→LUMO	MLCT/LLCT	0.15	435	420
Cu6	HOMO→LUMO	MLCT/LLCT	0.19	407	414
Cu7	HOMO→LUMO	MLCT/LLCT	0.17	403	410
Cu8	HOMO→LUMO	MLCT/LLCT	0.23	400	409

Table S3. The maximum emission wavelengths under different f_w for complex **Cu1** and **Cu6**.

f_w in the mixture (CH_3CN/H_2O)	Emission (λ_{max}, nm)	
	complex **Cu1**	complex **Cu6**
0%	515	542
10%	515	542
20%	515	542
30%	515	544
40%	515	544
50%	515	542
60%	520	544
70%	520	544
80%	555	554
90%	558	554

Table S4. The maximum emission wavelengths of complexes **Cu1** and **Cu6** in the presence of different metal ions.

Complexes in the presence of different metal ions	Emission (λ_{max}, nm)	
	Complex **Cu1**	Complex **Cu6**
Blank	560	567
Hg^{2+}	550	552
Zn^{2+}	558	560
Cd^{2+}	556	561
Na^{+}	556	564
Ag^{+}	562	560
Pb^{2+}	562	564
Mg^{2+}	559	561
Ni^{2+}	560	563
Cu^{2+}	560	561
Co^{2+}	559	564
Ba^{2+}	560	567
Ca^{2+}	565	565
Fe^{2+}	562	565
Fe^{3+}	563	569
Mn^{2+}	560	561
Li^{+}	565	563
Cr^{3+}	563	564